On the Spatial Propagation of Transient Magnetic Fields in AC Machines

Joachim Holtz, *Fellow, IEEE*
University of Wuppertal,
42097 Wuppertal – Germany

Abstract — **AC Motors have proliferated as the most important machine type used in speed variable drive systems. The dynamic analysis and description of revolving field machines is supported by well-established theories: Park's transformation (1929), and the space vector theory by Kovács and Rácz (1959). Yet some inconsistencies with the theory of dynamic systems exist: The machine eigenvalues suggest the existence of two damped oscillators; It appears unsatisfactory that the respective eigenfrequencies change with the velocity of the reference frame. This contradicts the common understanding according to which the eigenfrequency is an inherent system property.**

A clarification is reached using a novel approach for the dynamic analysis. The approach is based on complex state variables. It permits relating a transient condition to the propagation processes in space of distributed magnetic fields. The formal analysis constitutes an extension to the space vector theory and to the theory of dynamic systems.

1. Introduction

A clear and comprehensive description of the dynamic behaviour of ac machines is a fundamental requirement for their application in speed or torque controlled drive systems. The pertaining methods of dynamic analysis have been developed decades ago. They form part of the fundamentals in electrical engineering, being documented in numerous publications and books of reputed authors, [1] through [7].

2. Machine Equations

The dynamic analysis of ac machines is usually based on the following assumptions:

- Space harmonics of the flux linkage distribution are neglected,
- linear magnetics are assumed and iron losses are neglected, and
- slot harmonics and deep bar effects are not considered.

2.1 Park's transformation

The first comprehensive approach to the dynamic analysis of synchronous machines was contributed by *Park* [1]. The method was extended by *Kron* [2] to be applicable to any type of ac machine. The approach eliminates the redundancy of polyphase windings, substituting these by their two-axes equivalent. This reduces a polyphase winding to a set of two phase-windings having their magnetic axes arranged in quadrature as shown in Fig. 1. The two-axes representation eliminates the mutual magnetic coupling of the phase-windings, rendering the magnetic flux linkage of one winding independent of the current in the other winding. In a second step, both polyphase windings in the stator and the rotor of an ac machine are viewed from a common frame of reference which is either fixed to the stator, or to the rotor. More generally, the reference frame can be considered rotating at any arbitrary angular velocity ω_k.

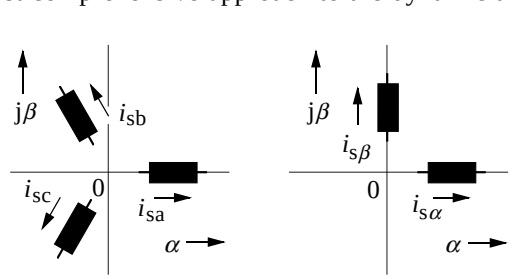

Fig. 1: Polyphase winding and two-axes equivalent

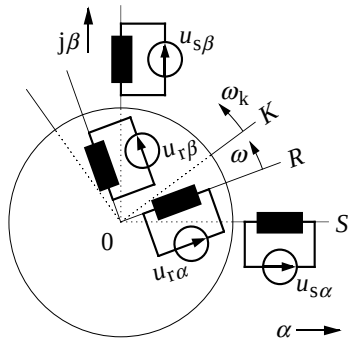

Fig. 2: Two-axes representation of an ac machine. *S, R, K,* denote the real axes of the stationary, the rotor-fixed, and the general coordinate system, respectively.

The common coordinate system is further interpreted as the complex plane, its real axis being denoted as the direct axis (*d*-axis), and the imaginary axis as the quadrature axis (*q*-axis).

According to *Kron*, a general ac machine is symbolically represented by the equivalent circuit Fig. 2. The general *k*-coordinate system rotates at the angular velocity ω_k with respect to the stator windings. The stator voltage equations, referred to the *k*-coordinate system, are expressed in terms of normalized quantities:

$$u_{sd} = r_s i_{sd} + \frac{d\psi_{sd}}{d\tau} - \omega_k \psi_{sq} \tag{1a}$$

$$u_{sq} = r_s i_{sq} + \frac{d\psi_{sq}}{d\tau} + \omega_k \psi_{sd} \tag{1b}$$

The angular mechanical velocity of the rotor is ω. As seen from the rotor, the *k*-coordinate system rotates at $\omega_k - \omega$, and hence the rotor voltage equations are

$$0 = r_r i_{rd} + \frac{d\psi_{rd}}{d\tau} - (\omega_k - \omega)\psi_{rq} \tag{1c}$$

$$0 = r_r i_{rq} + \frac{d\psi_{rq}}{d\tau} + (\omega_k - \omega)\psi_{rd} \tag{1d}$$

The flux linkages are proportional to the currents:

$$\psi_{sd} = l_s i_{sd} + l_h i_{rd} \quad (2a) \qquad \psi_{sq} = l_s i_{sq} + l_h i_{rq} \quad (2b)$$

$$\psi_{rd} = l_h i_{sd} + l_r i_{rd} \quad (2c) \qquad \psi_{rq} = l_h i_{sq} + l_r i_{rq} \quad (2d)$$

Note that all variables, like currents, voltages and flux linkages, have the property of scalars. Time is normalized throughout this paper: $\tau = \omega_{sR} t$, where ω_{sR} is the rated stator frequency.

It is particularly expedient to represent the foregoing system equations in a matrix notation, a technique which was decidedly promoted by *Kron* [3]. It leads to the general state equation

$$\dot{\boldsymbol{x}} = \boldsymbol{A}\boldsymbol{x} + \boldsymbol{B}\boldsymbol{u}, \quad (3)$$

where $\boldsymbol{A}$ is the n x n system matrix, $\boldsymbol{B}$ is the n x m input matrix, $\boldsymbol{u}$ contains the m x 1 forcing functions, and n is the system order. The state of the system is completely described by a set of state variables, contained in the n x 1 state vector $\boldsymbol{x}$.

2.2 The space vector notation

The absence of space harmonics, a precondition of the previous approach, signifies a rotating sinusoidal flux density distribution along the airgap. According to *Kovács* and *Rács* [4], a revolving field of such nature can be represented by a space vector. The space vector points to the maximum of the flux density wave as shown in Fig. 3; it expresses the maximum flux density value by its magnitude. Assuming that the rotor currents are zero, the flux density is proportional to the exciting currents in the stator winding. Consequently, these currents can be formally represented by a space vector. Considering a three-phase winding we have

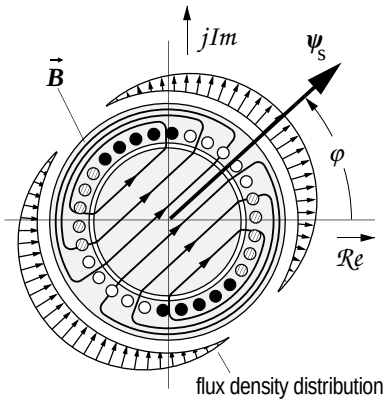

Fig. 3: Definition of a space vector (the rotor currents are assumed zero)

$$\boldsymbol{i}_s = \frac{2}{3}\left(i_a + a i_b + a^2 i_c\right), \quad (4)$$

where the respective coefficients 1, $a = exp(j2\pi/3)$, and a^2 of the three winding currents i_a, i_b and i_c are unity vectors indicating the spatial orientation of the respective winding axes.

According to *Kovács* and *Rács*, it is the proportionality between voltages and currents which justifies the definition of a voltage space vector in a similar way,

$$\boldsymbol{u}_s = \frac{2}{3}\left(u_a + a u_b + a^2 u_c\right), \quad (5)$$

where u_a, u_b and u_c are the respective phase voltages. Equations (4) and (5) effectively express the two-axes transformation of the respective three-phase quantities. The transformed variables are used to establish the voltage equations of an ac machine in terms of space vectors:

$$\boldsymbol{u}_s = r_s \boldsymbol{i}_s + \frac{d\boldsymbol{\psi}_s}{d\tau} + j\omega_k \boldsymbol{\psi}_s \quad (6a)$$

$$0 = r_r \boldsymbol{i}_r + \frac{d\boldsymbol{\psi}_r}{d\tau} + j(\omega_k - \omega)\boldsymbol{\psi}_r \quad (6b)$$

Given the proportionality between current and flux, the flux linkage space vectors are formally defined through the current vectors:

$$\boldsymbol{\psi}_s = l_s \boldsymbol{i}_s + l_h \boldsymbol{i}_r \quad (7a)$$

$$\boldsymbol{\psi}_r = l_h \boldsymbol{i}_s + l_r \boldsymbol{i}_r \quad (7b)$$

To sum up, the space vector notation as introduced by *Kovács* and *Rács* represents the sinusoidal field by a complex vector. It is postulated that the causes and the effects of such field, namely the currents and voltages, also have the property of space vectors owing to existing formal proportionalities.

2.3 Signal flow diagram

Equations (6) and (7) can be decomposed into their real and imaginary parts and rearranged as

$$\tau_s' \frac{d\psi_{sd}}{d\tau} + \psi_{sd} = \omega_k \tau_s' \psi_{sq} + k_r \psi_{rd} + \tau_s' u_{sd} \quad (8a)$$

$$\tau_s' \frac{d\psi_{sq}}{d\tau} + \psi_{sq} = -\omega_k \tau_s' \psi_{sd} + k_r \psi_{rq} + \tau_s' u_{sq} \quad (8b)$$

$$\tau_r' \frac{d\psi_{rd}}{d\tau} + \psi_{rd} = (\omega_k - \omega)\tau_r' \psi_{rq} + k_s \psi_{sd} \quad (8c)$$

$$\tau_r' \frac{d\psi_{rq}}{d\tau} + \psi_{rq} = -(\omega_k - \omega)\tau_r' \psi_{rd} + k_s \psi_{sq} \quad (8d)$$

where $\tau_s' = \sigma\tau_s$ and $\tau_r' = \sigma\tau_r$ are the transient time constants of the stator winding and the rotor winding, respectively, $k_s = l_h/l_s$ and $k_r = l_h/l_r$ are the magnetic coupling factors, and $\sigma = 1 - l_h^2/l_s l_r$ is the total leakage coefficient. Equations (8) can be also derived from (1) and (2). Their representation in graphic form is the signal flow diagram of the real state variables, Fig. 4. The graph demonstrates the strong intercoupling between the four electromagnetic state variables ψ_{sd}, ψ_{sq}, ψ_{rd}, ψ_{rq}. The complexity of this graph makes its interpretation almost impossible [5], [6].

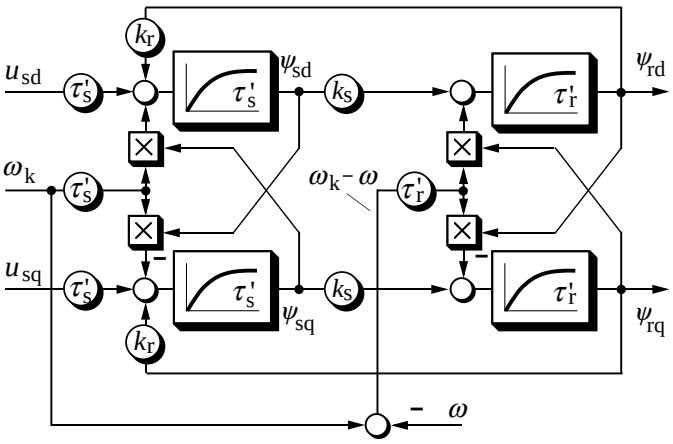

Fig. 4: Induction motor signal flow diagram (real state variables)

3. Discussion of AC Machine Dynamics

3.1 General

The behavior of a dynamic system during a general state of dynamic transition depends on the forcing function, and on its eigenbehavior. Supposing that the system is stable, its eigenbehavior in a given steady-state operating point is expressed by the particular way in which the state variables return to their respective steady-state values after a sudden displacement. The forcing functions must be left unchanged so as to maintain the steady-state condition. A displacement can be effected by adding a unit pulse to the steady-state forcing function; the deviation from the steady-state operating point it then described by the pulse response of the system in that very operating point.

The unit pulse transfers a determined amount of additional energy to the system. This energy is temporarily deposited in the storage elements of the system, for example those shown in Fig. 4; the energy then decays in the course of a subsequent transient, being partly dissipated as system losses, and partly absorbed by the load. This energy can be termed as transient energy, to be distinguished from the flow of steady-state energy which remains constant throughout the transient process.

Transient energy may either decay asymptotically, or, if a mutual coupling exists between two storage elements of different physical nature, oscillate between them. Such oscillation eventually fades away as the transient energy dissipates. In the root locus plane, the asymptotic decay is characterized by one negative real eigenvalue, whereas the oscillatory decay corresponds to a conjugate complex pair of eigenvalues having negative real parts.

3.2 Root locus plot

Apart from the signal flow diagram, another way of visualizing the properties of a dynamic system is the root locus plot. It is obtained with reference to (3) from the solution of

$$\boldsymbol{A}(\boldsymbol{\lambda} - \boldsymbol{I}) = 0\,, \qquad (9)$$

where $\boldsymbol{I}$ is the n x n identity matrix. The result is the n x 1 eigenvector $\boldsymbol{\lambda}$, the elements of which are the roots of the characteristic equation.

The following analysis concentrates on the electromagnetic subsystem of an induction motor, not considering the influence of the mechanical system. The mechanical time constant is therefore assumed very large, which renders the angular mechanical velocity ω = const.

The root locus plot of the electromagnetic subsystem as viewed from the stationary reference frame is shown in Fig. 5(a) with the angular mechanical velocity ω as a parameter. The plot exhibits two pairs of conjugate complex eigenvalues which suggest the existence of two oscillators [5]. The suggestion is supported by the particular structures in Fig. 4 that interconnect the stator state variables ψ_{sd} and ψ_{sq}, and, as a separate arrangement, the rotor state variables ψ_{rd} and ψ_{rq}. The respective structures are formed by series connections of two first-order delay systems in a negative feedback loop, which can indeed exhibit an oscillatory response.

In the root locus plot Fig. 5(a), the imaginary part of each pair of eigenvalues represents the eigenfrequency, and the real part controls the damping of the associated oscillator. Surprisingly, these eigenvalues are getting displaced to different locations when viewing the machine from a rotating reference frame, Fig. 5(b). This observation contradicts the common understanding according to which the eigenfrequency is an inherent property of a system. Such inconsistency can be explained to some extent: The change of reference frame entails a frequency transformation, not only of the feeding voltages and currents, but also of the machine generated transients. However, a better way of treating this problem is to avoid such ambiguities. This requires a distinctive approach which will be presented next.

4. The Complex State Variable Approach

4.1 Basic observations

Each pole of the root locus plot is uniquely associated with one energy storage element of the system under consideration. The storage element can be an inductor which stores the energy in its magnetic field; it can be the rotor of a machine and its kinetic energy at nonzero speed.

A pair of conjugate complex poles represents two independent storage elements of different physical nature which, in a state of dynamic excitation, exchange their energy periodically in the form of an oscillation. The frequency depends on the storage capacities of the two elements; it is an inherent system property.

Such oscillator can be formed, for example, by paralelling a capacitor to an inductor. The magnetic energy of the inductor transfers to the capacitor, being temporarily stored

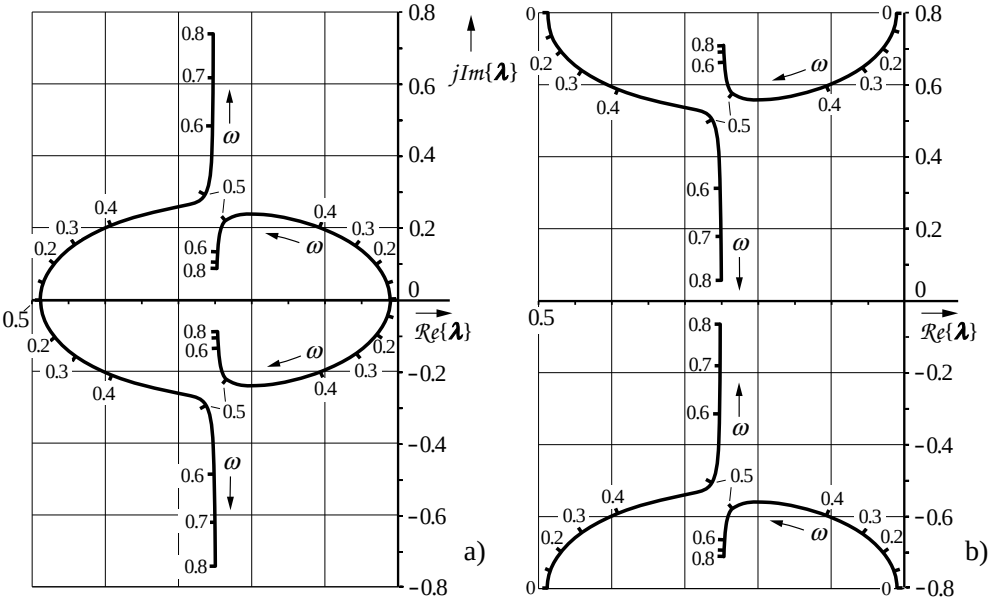

Fig. 5: Root locus plot of the electromagnetic subsystem, (a) stator coordinates, (b) rotating coordinates

as electrical energy, and then retransfers in the course of an oscillation. Similarly, a torsional spring can temporarily absorb the transient kinetic energy of a rotating mass, thus assisting to sustain a damped mechanical oscillation.

Different from these examples, revolving field machines define a class of dynamic systems for which the foregoing interpretation does not unconditionally apply. A polyphase winding in its two-axes representation is characterized by two energy storage elements. Both are inductances, and as such cannot interact to sustain independent oscillations. This legitimates representing the magnetic energy of a polyphase winding as one entity, not to be devided into portions attributed to the respective axes. The approach requires a second degree of freedom which is the spatial orientation of the magnetic field that represents the total energy. Reasoning from that, the traditional space vector is well suited to serve as the single state variable to represent an entire winding.

4.2 Current space vectors

The use of complex state variables for the dynamic analysis requires a more rigid definition of a space vector than that originally given by *Kovács* and *Rács* [4]; their definition is discussed in Section 2.2. It is not only the revolving flux density wave that is sinusoidally distributed around the airgap. Also the mmf of each phase winding has the same distribution, which follows from the initial assumptions in Section 2. This means that the conductors pertaining to one phase must have a sinusoidal density distribution along the airgap, producing a sinusoidal mmf distribution. Such distribution can be represented by a space vector. The defintion of an mmf space vector, being directed in space towards the maximum mmf density of the phase winding, is not very practical. An equivalent current vector is therefore preferred which lags the mmf space vector by 90° in space. It points in the direction of the winding axis, thus being aligned with the flux linkage component that is produced by the winding current. The magnitude of the current space vector is directly related to the respective phase current at the winding terminals.

In a polyphase winding, each phase winding generates a sinusoidal mmf distribution, to which a phase-current space vector is attributed (which is different from the current space vector of the polyphase winding). In a three-phase winding, the phase-current space vectors are $\underline{1}\cdot i_a$, $a i_b$, and $a^2 i_c$, respectively, where $\underline{1} = exp(j0)$. The total mmf distribution of all phase currents is the superposition of the respective sinusoidal mmf profiles; the distribution is represented by a current space vector, expressed in (4) as the sum of the contributing phase-current space vectors.

4.3 Voltage space vectors

With the conductors of a phase winding being arranged in a sinusoidal density distribution around the airgap, the local resistive voltage drop created by the winding current varies in proportion to the winding density. This voltage assumes a sinusoidal distribution in space to which a voltage space vector is assigned. The same applies to the induced voltage that originates from changes of the flux linkage. The total phase voltage builds up as the sum of its distributed increments and equals the magnitude of the phase-voltage space vector. A three-phase winding contributes the phase-voltage space vectors $\underline{1}\cdot u_a$, $a u_b$, and $a^2 u_c$. They sum up geometrically to the voltage space vector of the polyphase winding according to (5).

4.4 Winding representation

Apart from an arrangement of distributed conductors, a phase winding can be made up from concentrated coils on salient magnetic poles. The field winding in the rotor of a synchronous machine is an example. It generates a spatial flux density distribution which is sinusoidal by virtue of an appropriately shaped airgap, and hence it can be represented by a flux linkage space vector $\boldsymbol{\psi}_f$, Fig. 6(a). Assuming that all other machine windings have zero currents, the voltage equation in rotor coordinates,

$$\tau_f \frac{d\boldsymbol{\psi}_f}{d\tau} + \boldsymbol{\psi}_f = \tau_f \boldsymbol{u}_f, \tag{10}$$

characterizes the winding dynamically as a first order system having the complex state variable $\boldsymbol{\psi}_f$, and the time constant $\tau_f = l_f/r_f$. The phase angle of the flux linkage wave is identical to the rotor position angle φ. In rotor coordinates, the flux linkage vector is invariably aligned with the real axis. $d\boldsymbol{\psi}_f/d\tau$ is a distributed voltage which transforms to a scalar dc voltage at the machine terminals, with the relative position of the slip ring brushes contributing the phase transformation angle. The signal flow graph in the center of Fig. 6(a) is the dynamic representation of (10). It refers to the winding-fixed, i. e. the rotor coordinate system. Shown in the bottom of Fig. 6(a) is the eigenvalue of (10).

An identical airgap flux density wave can be generated by a polyphase winding in the stator, Fig. 6(b). The spatial orientation of the stator flux linkage can assume any angular orientation, depending on the magnitudes of the respective phase currents. As before, the currents in other machine

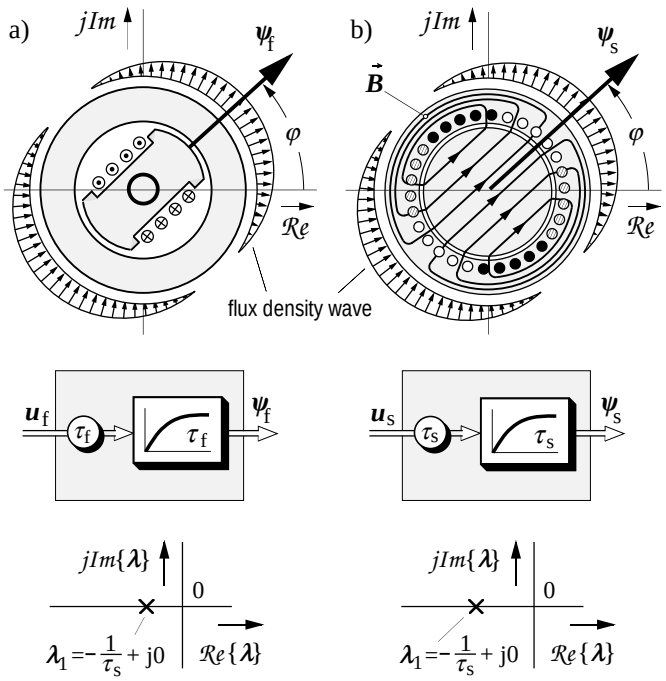

Fig. 6: Complex notation of machine windings. (a) salient rotor winding, (b) polyphase stator winding. From top to bottom: winding geometry and flux linkage vectors; signal flow graphs; root loci

windings are assumed zero. Referring again to a coordinate system that is stationary with respect to the winding leads to

$$\tau_s \frac{d\boldsymbol{\psi}_s}{d\tau} + \boldsymbol{\psi}_s = \tau_s \boldsymbol{u}_s \qquad (11a)$$

which is a first order delay having the complex state variable $\boldsymbol{\psi}_s$, and the time constant $\tau_s = -1/\mathcal{R}e\{\boldsymbol{\lambda}_1\}$. The equation underlines the inductive nature of the distributed winding. The dynamic structure is shown in the center of Fig. 6(b). The root locus is obtained from (9), where $\boldsymbol{A}$ is derived from the state space form of (11a). Fig. 6(b) shows that a single complex pole $\boldsymbol{\lambda}_1 = -1/\tau_s + j0$ exists.

A transformation of (11a) to the general *k*-coordinate system is formally effected by multiplying this equation by the rotation term $exp(j\omega_k)$:

$$\tau_s \frac{d\boldsymbol{\psi}_s}{d\tau} + \boldsymbol{\psi}_s = -j\omega_k \tau_s \boldsymbol{\psi}_s + \tau_s \boldsymbol{u}_s \qquad (11b)$$

The representation of the winding in a rotating reference frame adds the dynamically induced voltage $-j\omega_k \tau_s' \boldsymbol{\psi}_s$ to the system equation (11b). This term maps in the signal flow diagram Fig. 7(a) as an additional feedback loop around the complex delay element. The root locus plot Fig. 7(b) shows that the complex eigenvalue is now displaced by $-j\omega_k$ as compared with Fig. 6(b). The displacement indicates that the winding rotates at the angular velocity $-j\omega_k$ with respect to the coordinate system. The same information is conveyed in the signal flow diagram by the complex feedback term $-j\omega_k \tau_s' \boldsymbol{\psi}_s$.

4.5 Comparison

The complex state variable analysis produces results that differ from those of the real state variable notation. A comparison can be summarized as follows:

The analysis of a polyphase winding as represented in (1) by real state variables leads to a second-order system, which corresponds to an oscillator in the signal flow structure and, correspondingly, a pair of conjugate complex eigenvalues. Hence the transient response is characterized by a *time dependent oscillation*, the frequency of which depends on the coordinate system.

Against this, the complex state variable approach represents the winding as a first-order delay, the time constant of which is the *l*/*r*-ratio of the winding. The root locus shows a single complex eigenvalue without a conjugate complex correspondent. The imaginary part of the single complex eigenvalue represents the magnitude and the direction of the angular velocity at which the winding rotates against the coordinate system. Being based on one single complex eigenvalue, the transient response describes the *spatial displacement* of the transient energy that is associated to that state variable.

It is important to observe that the stored energy of the system is continuously spread out in space. Subdividing the energy into two portions that are formally described by the scalar real and imaginary parts of the corresponding space vector is an arbitrary manipulation. Such partition of energy depends on the phase angle of the reference frame which is not a system property and can be freely chosen. Introducing the real part and the imaginary part as system state variables attaches information to them that is alien to the system properties.

5. Transient Analysis

5.1 The electromagnetic subsystem

An induction motor comprises two polyphase windings, one located in the stator and one in the rotor. The system equations are derived from (6) and (7):

$$\tau_s' \frac{d\boldsymbol{\psi}_s}{d\tau} + \boldsymbol{\psi}_s = -j\omega_k \tau_s' \boldsymbol{\psi}_s + k_r \boldsymbol{\psi}_r + \tau_s' \boldsymbol{u}_s \qquad (12a)$$

$$\tau_r' \frac{d\boldsymbol{\psi}_r}{d\tau} + \boldsymbol{\psi}_r = -j(\omega_k - \omega)\tau_r' \boldsymbol{\psi}_r + k_s \boldsymbol{\psi}_s \qquad (12b)$$

The equations are visualized in the signal flow graph Fig. 8 as a complex second-order system. The two basic winding structures demonstrate that the stator winding rotates at the angular velocity $-\omega_k$, and the rotor winding rotates at $-\omega_r = -(\omega_k - \omega)$, with respect to the general ω_k coordinate system.

The root locus plot Fig. 9 shows that there are two single complex eigenvalues that get displaced as the mechanical angular velocity ω changes. It could be concluded that the stretched eigenvalue curve on the left represents the rotor winding, since its imaginary part increases almost in proportion to the rotor speed. This leaves the right-hand side curve for the stator winding, a less convincing conclusion in view of the strong rotational component that governs the imaginary part of the associated root in the medium speed range.

Closer insight into the problem is gained by looking at the propagation in space of the magnetic energy associated to the windings. The spatial distributions are described by the respective flux linkage vectors $\boldsymbol{\psi}_s$ and $\boldsymbol{\psi}_r$.

It is assumed as a general initial condition that the machine operates in the steady-state at arbitrary values of stator voltage and stator frequency. The angular mechanical speed ω then adjusts as determined by the load torque. A

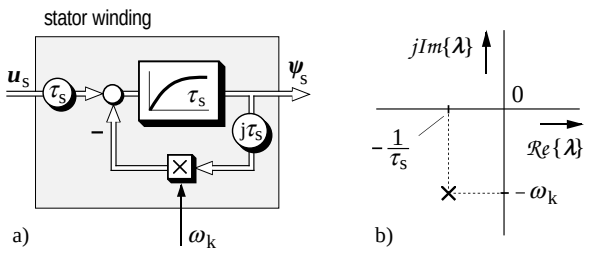

Fig. 7: Polyphase stator winding in rotating coordinates, (a) signal flow graph, (b) root locus

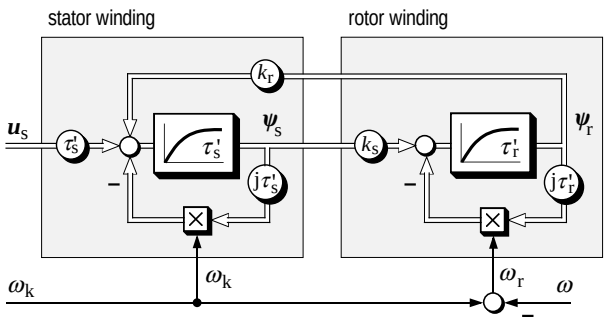

Fig. 8: Induction motor signal flow graph in terms of complex state variables

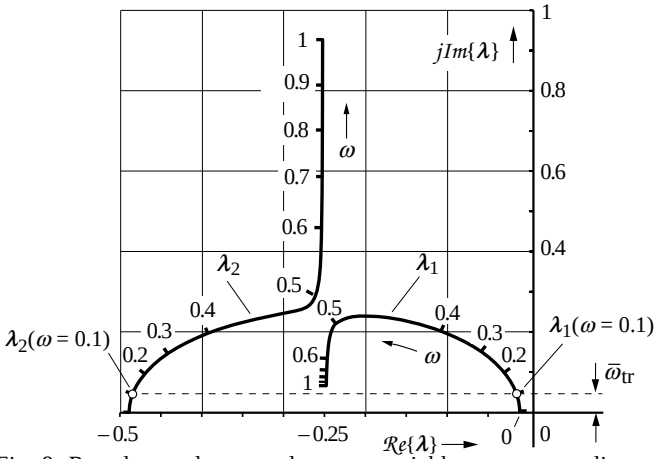

Fig. 9: Root locus plot, complex state variables, stator coordinates; the circles mark the eigenvalue locations at $\omega = 0.1$.

transient process is subsequently stimulated by superimposing a unit pulse $\boldsymbol{\delta}(\tau = 0) = 0 + \mathrm{j}$ to the stator voltage vector. The response is obtained as the solution of the system equations (12) as

$$\check{\boldsymbol{\psi}}_\mathrm{s} = \frac{1}{\boldsymbol{\xi}\tau_\mathrm{r}'}\left[\begin{array}{l}\frac{1}{2}\tau_\mathrm{r}'\left(\boldsymbol{\lambda}_1 exp(\boldsymbol{\lambda}_1\tau) - \boldsymbol{\lambda}_2 exp(\boldsymbol{\lambda}_2\tau)\right) \\ +\left(1-\mathrm{j}\omega\tau_\mathrm{r}'\right)exp\left(-\frac{1}{2}\boldsymbol{\zeta}\tau\right)sinh(\boldsymbol{\xi}\tau)\end{array}\right] \qquad (13a)$$

$$\check{\boldsymbol{\psi}}_\mathrm{r} = \frac{k_\mathrm{s}}{\boldsymbol{\xi}\,\tau_\mathrm{r}'}exp\left(-\frac{1}{2}\boldsymbol{\zeta}\tau\right)sinh(\boldsymbol{\xi}\tau), \qquad (13b)$$

where $$\boldsymbol{\zeta} = \frac{(1-\mathrm{j}\omega\tau_\mathrm{r}')}{\tau_\mathrm{r}'} + \frac{1}{\tau_\mathrm{s}'} \qquad (13c)$$

and

$$\boldsymbol{\xi} = \sqrt{\left(\frac{r_\mathrm{s}'(1-\mathrm{j}\omega\tau_\mathrm{r}') + r_\mathrm{r}'}{2\,r_\mathrm{s}'r_\mathrm{r}'}\right)^2 - \frac{1-\mathrm{j}\omega\tau_\mathrm{r}' - k_\mathrm{s}k_\mathrm{r}}{\tau_\mathrm{s}'\tau_\mathrm{r}'}}\,. \qquad (13d)$$

The space vectors $\check{\boldsymbol{\psi}}_\mathrm{s}$ and $\check{\boldsymbol{\psi}}_\mathrm{r}$ describe the transient deviation from a steady-state operating point characterized by $\boldsymbol{\psi}_\mathrm{s}$ and $\boldsymbol{\psi}_\mathrm{r}$. Hence the total flux linkages during a transient are $\boldsymbol{\psi}_{\mathrm{s\,total}} = \boldsymbol{\psi}_\mathrm{s} + \check{\boldsymbol{\psi}}_\mathrm{s}$, and $\boldsymbol{\psi}_{\mathrm{r\,total}} = \boldsymbol{\psi}_\mathrm{r} + \check{\boldsymbol{\psi}}_\mathrm{r}$. The superposition is permitted since the system is considered linear (ω, ω_k = const.).

The transient deviations $\check{\boldsymbol{\psi}}_\mathrm{s}$ and $\check{\boldsymbol{\psi}}_\mathrm{r}$ will be now discussed for different values of the angular mechanical velocity ω.

Fig. 10 shows on its left-hand side how the trajectories of the transient flux linkage vectors $\check{\boldsymbol{\psi}}_\mathrm{s}$ and $\check{\boldsymbol{\psi}}_\mathrm{r}$ develop in a time sequence. Their locations are displayed immediately after the exciting pulse occurs, and then after a quarter revolution, and again after half a revolution of the rotor. The pertaining schematic field patterns on the right-hand side illustrate how the transient magnetic energy distributes in space.

The field patterns extend over one pole pair of the machine. The circumferential airgap had been opened out to become linear and given an extended width for a better demonstration of the important field distribution details in the airgap space. The conductors of the polyphase windings in the stator and the rotor can be imagined as layers of infinite thickness being located along the boundaries between the active iron and the airgap.

It is particularly important to note that the spatial flux distributions in Fig. 10(b), as well as those in the following figures, have been simply drawn by hand using a computer mouse. There was no numerical field computation program used for this purpose. The information contained in the respective field patterns is only that conveyed by the solution (13) of the system equations. The solution provides the sinusoidal distributions along the boundaries to the active iron on both sides of the airgap. These distributions are completely described by the respective magnitudes and phase angles of the transient components of the stator flux linkage vector and the rotor flux linkage vector.

The spatial distributions in the airgap volume have been subsequently completed by applying the fundamental rules that hold for the behavior of magnetic fields in the neighborhood of boundaries between different magnetic materials. The validity of the obtained results, though, was confirmed by numerical field computation.

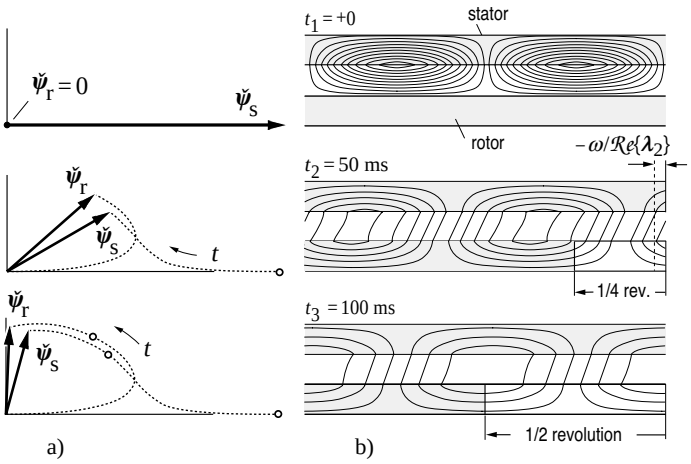

Fig. 10: Time sequence of transient magnetic fields at $\omega = 0.1$, (a) locations of the flux linkage vectors, (b) field distributions

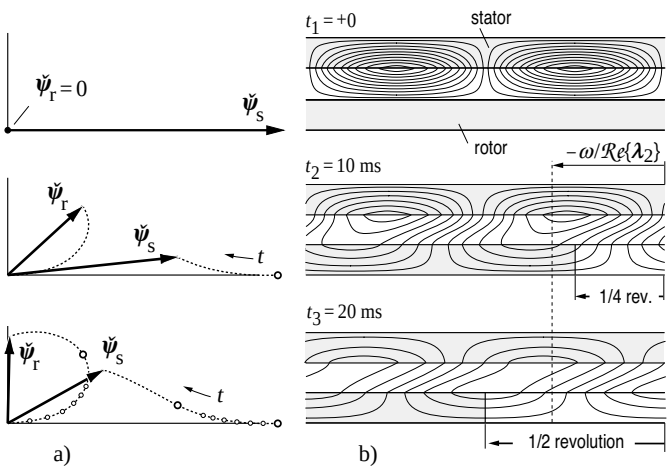

Fig. 11: Time sequence of transient magnetic fields at $\omega = 0.5$, (a) locations of the flux linkage vectors, (b) field distributions

5.2 Transient response at low speed

Low speed operation is defined as $\omega < |1/\mathcal{R}e\{\boldsymbol{\lambda}_2(\omega = 0)\}|$. As an example, $\omega = 0.1$ is selected in Fig. 10. At $t_1 = +0$, a defined amount of transient energy is injected through the stator terminals by a complex unit pulse that is superimposed to the steady-state stator voltage vector. The transient energy is stored in a magnetic field that links exclusively with the stator winding, and hence is categorized as a leakage field. This field does not link with the rotor windings since the initial transient rotor flux linkage is zero. Rotor currents are instantaneously induced by the sudden appearance of the transient stator flux linkage. They repel the flux linkage from the rotor. Owing to the presence of such rotor currents, the rotor resistance gets transformed to the equivalent stator circuit and influences the effective transient time constant.

The leakage field closes through the airgap, pervading the large distance of about a pole pitch in the circumferential direction. The high magnetic resistance of this particular path makes the transient inductance of the stator winding very low. Hence the transient time constant $\tau_2'(\omega = 0.1) = -1/\mathcal{R}e\{\boldsymbol{\lambda}_2(\omega = 0.1)\}$ is small.

As time elapses, the initial situation changes very rapidly. This is illustrated in the center portion of Fig. 10(b) at $t_2 = 50$ ms. The rotor has just executed a quarter revolution at this instant of time. The displacement angle $\omega \cdot \tau_2'(\omega = 0.1) = -\omega/\mathcal{R}e\{\boldsymbol{\lambda}_2(\omega = 0.1)\}$ marked on the right indicates that the transient time constant τ_2' has elapsed long before completion of the first quarter revolution. Hence the leakage field through the airgap has faded away almost completely. The resistive rotor voltage drop has assisted to build up a rotor flux linkage. That flux component has reached by now almost the same magnitude as the transient flux linkage in the stator. This is demonstrated by the space vector diagram on the left of Fig. 10(b). The corresponding field pattern on the right shows a strong mutual flux linkage. The airgap is intersected almost at shortest distance, from which a high winding inductance, and consequently a large time constant results. The mutual field will therefore persist over a longer period of time; it has not very much reduced after another quarter revolution as illustrated in the lower portion of Fig. 10(b).

The propagation velocity ω_{tr} of the transient fields can be numerically extracted from (13), which represent the dotted trajectories of the flux linkage vectors in Fig. 10(a). Shortly after their initialization, both flux linkage vectors displace at the constant velocity $\omega_{tr} = \omega/2$. This is confirmed by the imaginary parts of the respective eigenvalues in Fig. 9. Both equal the time-averaged value $\overline{\omega}_{tr} = Im\{\boldsymbol{\lambda}_1(\omega)\} = Im\{\boldsymbol{\lambda}_2(\omega)\} = 0.5\,\omega = 0.05$ as indicated by the dashed horizontal line in Fig. 9. The real parts of the two eigenvalues equal the inverse time constants which control the decay of the leakage flux linkage, and the mutual flux linkage, respectively. The field distributions show that the stator field displaces in a positive direction with respect to the stator, and the rotor field in a negative direction with respect to the rotor. As seen from the common stationary reference frame, both fields displace in the time average at $\overline{\omega}_{tr}$ as expressed by the imaginary components of their eigenvalues.

5.3 Transient response at medium speed

The conditions of transient field propagation change at higher speed. The particular machine investigated here (the data are given in the Appendix) obviously exhibits unique operating conditions around $\omega = 0.5$, a region where the two branches of the root locus plot in Fig. 9 have their minimum distance and maximum curvature. As a general rule for any machine, this condition prevails at $\omega \approx 1/\mathcal{R}e\{\boldsymbol{\lambda}_2(\omega = 0)\}$.

The particular situation at $\omega = 0.5$ is assessed from the details in Fig. 11(b). Following the injection of transient energy, the transient field again penetrates from the stator into the rotor, but slower than in the previous case. This can be demonstrated by the evaluation of (13). The fact is confirmed by the value $\mathcal{R}e\{\boldsymbol{\lambda}_2\}$, the negative inverse of which is the time constant of the transient leakage field, $\omega \cdot \tau_2'(\omega = 0.5) = -\omega/\mathcal{R}e\{\boldsymbol{\lambda}_2(\omega = 0.5)\}$. A visual inspection confirms that the rotor flux linkage trajectory has a different shape than the corresponding one in Fig. 10. The field pattern in the center portion of Fig. 11 shows that, contrasting to the situation in Fig. 10, a leakage flux still exists after a quarter revolution. This is necessarily so, since the rotor has not yet displaced to the angular position $\omega \cdot \tau_2'(\omega = 0.5)$, which it will only reach when the transient time constant $\tau_2'(\omega = 0.5)$ has elapsed.

A mutual flux linkage has meanwhile established. Since the rotor moves faster than in the previous case, the mutual airgap field develops a strong circumferential component. At this higher speed the respective transient flux linkages develop a tendency to adhere to their respective windings. As a consequence, the mechanical displacement between the stator and the rotor does not entail proportionate displacements of the stator flux linkage relative to the stator, and of the rotor flux linkage relative to the rotor. Hence the phase angle between the pertinent space vectors must increase.

Although most of the mechanical displacement between the stator and the rotor is compensated by respective displacements of the stator flux linkage and the rotor flux linkage, the phase angle between the pertinent space vectors increases. The resulting elongation of the airgap flux lines increases the magnetic resistance encountered by the mutual flux. Hence the time constant of the mutual flux linkage decreases. The flux patterns further reveal that the magnetic resistances of the leakage flux linkage and the mutual flux linkage are almost the same, a fact which is confirmed by the real parts of their respective root loci at $\omega = 0.5$, Fig. 12.

The velocity at which the transient magnetic fields displace along the airgap is expressed by the angular velocity of the flux linkage vectors. The respective values are ob-

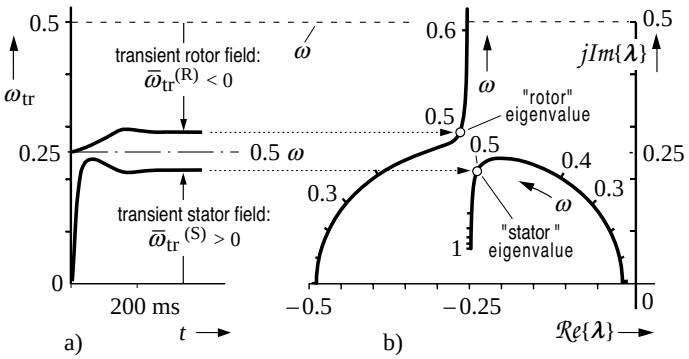

Fig. 12: Velocity of transient fields and eigenvalue location at medium speed, $\omega = 0.5$; (a) velocity versus time, (b) location of root loci

tained from a numerical simulation and plotted as time functions in Fig. 12(a). The stator flux linkage velocity starts from zero and increases in proportion as the rotor field builds up in magnitude. Interestingly, the initial rotor field velocity equals $\omega/2$ although the rotor flux linkage is still zero at $t = 0$, a fact that is difficult to confirm just from the shape of the trajectories of the flux linkage vectors in Fig. 11. The velocities of these vectors settle after a short oscillation to reach their respective steady-state values, Fig. 12(a). The comparison with the root loci in Fig. 12(b) shows that the steady-state velocity of the transient fields equals the imaginary parts of the respective system eigenvalues:

$$\overline{\omega}_{\mathrm{tr}1,2} = Im\{\boldsymbol{\lambda}_{1,2}\} \tag{14}$$

It can be again observed that the velocity of the transient stator field with respect to the stator equals the velocity of the transient rotor field with respect to the rotor. Other than at lower speed (Section 5.2), the velocities of the transient fields relative to their windings do not sum up to the mechanical speed of the rotor: there remains a gap between the two curves in Fig. 12(a). Hence the airgap flux lines in Fig. 11(b) continue to elongate throughout the transient process.

Note that the particular shape of the initial oscillation in the velocity curves in Fig. 12(a) is not related to a system eigenvalue, a quite peculiar obervation.

The speed range aroung $\omega = 1/\mathcal{R}e\{\boldsymbol{\lambda}_2(\omega = 0)\}$ marks a particular situation in which the mutual flux linkage has effectively decayed before the displacement angle between the stator and the rotor field has reached the extension of one pole pitch. This situation will not be encountered at higher speed.

5.4 Transient response at higher speed

A third case of interest is $\omega > \left|1/\mathcal{R}e\{\boldsymbol{\lambda}_2(\omega = 0)\}\right|$. In this upper speed range, the rotor completes more than a revolution before the leakage transients have died out. This is reflected in the trajectory of the rotor flux linkage vector in Fig. 13, which completes several circles in the complex plane before its transient energy has dissipated. It is of particular interest that the trajectory passes repeatedly through the origin. This happens approximately every two revolutions of the rotor. The mechanism behind is explained with reference to Fig. 14, which illustrates the spatial propagation of the transient fields at $\omega = 0.8$ in a time sequence.

At that speed, the induced rotor flux linkage is quickly carried away by the moving rotor winding, while the transient stator flux linkage remains almost stationary. Before the transient time constant $\tau_2'(\omega = 0.8)$ elapses, the rotor field has reached a position that is closer to the adjacent stator pole than to the original pole from which it had been

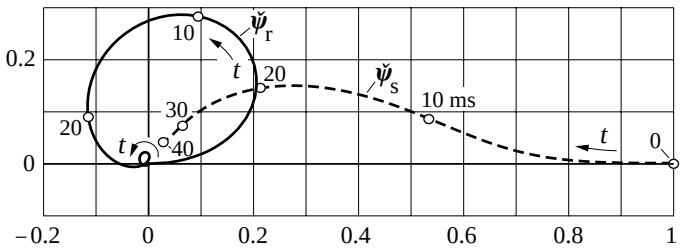

Fig. 13: Trajectories of the transient flux linkage vectors at medium speed; $\omega = 0.8$

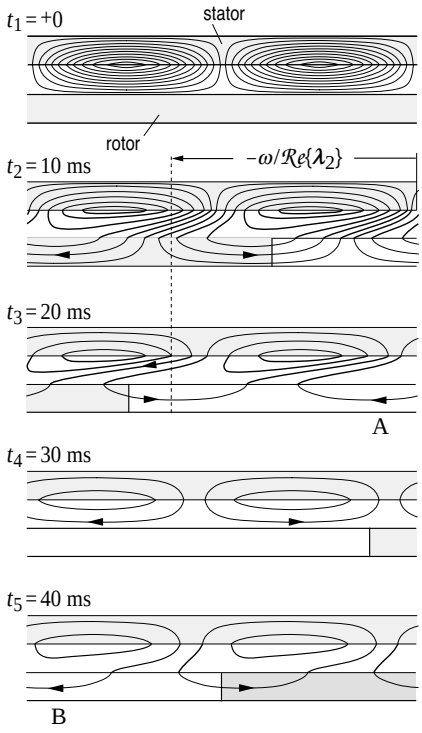

Fig. 14: Time sequence of transient magnetic fields at $\omega = 0.8$; for A and B see text

induced. While the magnetic field continues to penetrate from the stator, it gets displaced and becomes eventually opposed in direction to the existing rotor flux linkage. The magnitude of the rotor field therefore recedes, coming down to zero at $t_4 = 18$ ms in the example Fig. 4. The existing field distribution is then equivalent to the starting condition at $t_1 = +0$. Consequently, the penetration of the stator flux linkage into the rotor starts again, although at reduced magnitude since some of the transient energy has meanwhile been dissipated. Note that the rotor field, as seen in a given area of the rotor surface, has now established in a reversed direction as referred to its original polarity of magnetization.

The disappearance and reappearance of the rotor field is a cyclic process which is illustrated by the diagram Fig. 15. Initially, the angular velocity of the stator flux linkage in Fig. 15(a) increases as the rotor flux magnitude increases; it decreases again as soon as the rotor has displaced its flux linkage to oppose the stator flux linkage in polarity. The rotor field then reduces to a minimum value. The interaction with the stator almost discontinues, leaving the stator flux linkage nearly stationary. Effectively, the rotor field moves periodically much faster than the rotor winding. This happens whenever the large peaks in the rotor velocity curve

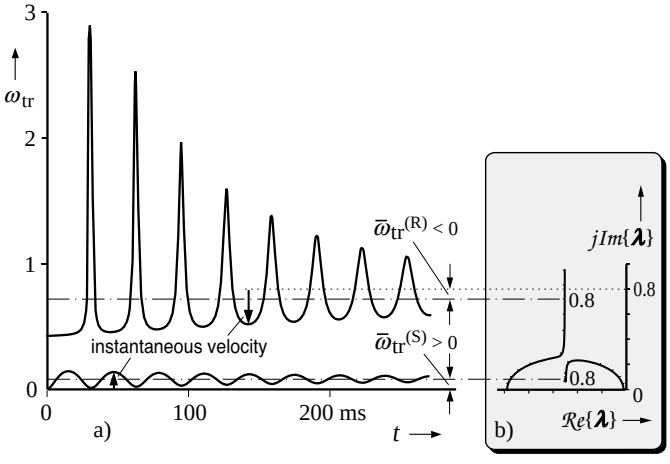

Fig. 15: Velocity of transient fields and eigenvalue location at higher speed, $\omega = 0.8$; (a) time functions, (b) root loci

occur, during which $\omega_{tr} >> \omega$. The field pattern Fig. 14 shows indeed that the rotor field distribution at $t = t_3$ (marked A) reappears in a much more advanced location B at $t = t_5$ when the field has build up again from zero.

During the following cycles, the velocity peaks reduce in magnitude. The average velocity $\overline{\omega}_{tr}$, however, remains constant; it equals the imaginary part of the rotor eigenvalue (14), which is is indicated by the appropriately scaled root locus plot in Fig. 15(b). Also the average stator field velocity is constant; it equals the imaginary part of the other eigenvalue.

Surprisingly, the frequency and the rate of decay of the velocity oscillations are not correlated to a system eigenvalue; their oscillations persist for a much longer duration than any of the machine eigenvalues would indicate.

The field patterns in Fig. 14 demonstrate that the magnetic path of the transient leakage field is shorter at $\omega = 0.8$ than that at very low speed, Fig. 10(b). Hence the transient time constant $\tau_2'(\omega = 0.8)$ can be expected to be larger. The opposite is true for the mutual field component: this field develops a strong circumferential component at $\omega = 0.8$, Fig. 14, which increases the magnetic resistance as compared with the low speed case. Accordingly, the corresponding transient time constant $\tau_1'(\omega = 0.8)$ must be smaller than at lower speed. The root locus plot Fig. 9 confirms that the two transient time constants, expressed as the inverse real parts of the corresponding eigenvalues, approach each other as the speed increases, finally assuming almost the same magnitudes at high speed.

5.5 The magnetic symmetry of the induction motor

It was demonstrated that the average velocity of the transient stator field relative to the stator equals the average velocity of the transient rotor field relative to the rotor. The fact suggests representing the two system eigenvalues in their respective reference frames. For this purpose, the rotor eigenvalue is transformed to rotor coordinates: $Im\{\lambda_2^{(S)}(\omega)\} = Im\{\lambda_2^{(R)}(\omega)\} - \omega$. Fig. 16 shows that the loci of these eigenvalues assume symmetric positions around a center point $-(1/\tau_s' + 1/\tau_r')/2$, [10].

Although apparently convenient, the association of a particular eigenvalue to either the stator or the rotor appears questionable as it holds only for certain speed ranges. It is in fact the leakage and the mutual transient field components, their velocities of propagation, and their rates of decay, that are reflected in two single complex roots. The state-of-the-art dynamic analysis of revolving field machines fails to provide such comprehensive insight.

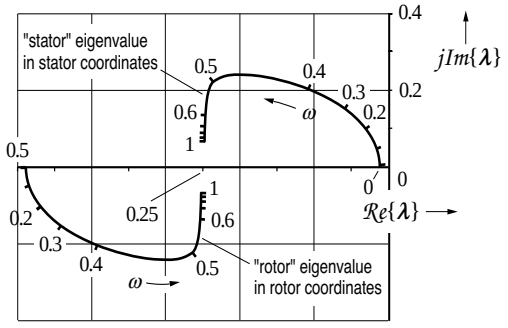

Fig. 16: Root loci of eigenvalues as referred to their respective coordinate systems

6. Conclusion

The dynamic analysis of ac machines is commonly based on real state variables. Conjugate complex pairs of eigenvalues describe the dynamic response as time-dependent oscillations. These determine the transient phase currents at the machine terminals and the related scalar flux linkages.

Different from that, the dynamic process inside the machine is characterized by continuous distributions in space of voltages, currents, and flux linkages. Their stringent representation by complex state variables discloses a more comprehensive description of the transient phenomena. It characterizes the electromagnetic subsystem of an ac machine by two single complex eigenvalues excluding their conjugate correspondents. The eigenvalues provide information on the velocities of the transient magnetic fields, and they also reveal the velocity of the reference frame.

The solution of the complex system equations are simple arithmentic expressions. Nevertheless, they provide every detail of the spatial distributions of transient magnetic fields in the active iron and in the airgap volume, equivalent to what can be obtained by numerical field analysis.

It is a particular appeal of the approach that it explains with unprecedented insight the physical significance of the root loci and the relationship of their locations to the time-varying spatial propagation of transient magnetic fields.

Acknowledgement: The author expresses his sincere thanks to Prof. R. Belmans, University of Leuven, Belgium, for doing the numerical field computations that are referred to in this paper.

7. Appendix

The investigated machine has the following data:
$l_s = 3.005$, $r_s = 0.0446$, $l_h = 2.89$, $l_r = 3.13$, $r_r = 0.054$.

8. References

1. R. H. Park, „Two-reaction theory of synchronous machines“, *Transactions AIEE*, 1929.
2. G. Kron, „A Short Course in Tensor Analysis for Electrical Engineers“, *John Wiley & Sons*, New York, 1942.
3. G. Kron, „Tensors for Circuits“, *Dover Publications Inc.*, New York, 1959.
4. P. K. Kovács and E. Rácz, „Transient Phenomena in Electrical Machines“, (in German), *Verlag der Ungarischen Akademie der Wissenschaften*, Budapest, 1959; English edition: *Elsevere Science Publishers*, Amsterdam, 1984.
5. W. Leonhard, „Control of Electrical Drives“, *Springer-Verlag, Berlin*, 1985.
6. A. Bühler, „Introduction to the Theory of Controlled Electrical Drives“, (in German), *Birkhäuser, Basel*, 1977.
7. P. C. Krause, O. Wasynczuk, S. D. Sudhoff, „Analysis of Electrical Machinery“, *IEEE Press*, 1994.
8. D. W. Novotny, J. H. Wouterse, „Induction Machine Transfer Functions and Dynamic Response by Means of Complex Time Variables“, *IEEE Trans. on Power Apparatus and Systems*, Vol. PAS-95, No. 4, July/August 1976, pp. 1325-1333.
9. K. Ogata, „State Space Analysis of Control Systems“, *Prentice Hall Inc.*, Englewood Cliffs, N.J., 1967.
10. J. Holtz, „The Representation of AC Machine Dynamics by Complex Signal Flow Graphs“, *IEEE Trans. on Industrial Electronis*, Vol. 42, No. 3, June 1995, pp. 263-271.